Electron nuclear double resonance spectroscopy of Cr^{3+} ions in potassium dihydrogen phosphate

1992 J. Phys.: Condens. Matter 4 2297

(http://iopscience.iop.org/0953-8984/4/9/023)

J. Phys.: Condens. Matter 4 (1992) 2297–2308. Printed in the UK

Electron nuclear double resonance spectroscopy of Cr^{3+} ions in potassium dihydrogen phosphate

D Bravo†, R Böttcher‡ and F J López†

† Departamento de Física Aplicada, C-IV, Universidad Autónoma de Madrid, Cantoblanco, E-28049 Madrid, Spain

‡ Sektion Physik, Universität Leipzig, 0-7010 Leipzig, Federal Republic of Germany

Received 14 August 1991

Abstract. The ENDOR spectra of Cr^{3+} ions in KDP have been measured at 4.2 K and the hyperfine interaction with the nearest neighbour protons has been investigated. The results confirm the EPR model for the defect: the Cr^{3+} substitutes for K^+ with two proton vacancies in the first shell. The relaxation of the lattice ion in the neighbourhood of the impurity is also discussed.

1. Introduction

Potassium dihydrogen phosphate (KDP) and its isomorphs have been actively investigated by a number of experimental techniques, as well as theoretically, and they have also attracted the interest of magnetic resonance spectroscopies. Most of the electron paramagnetic resonance (EPR) and electron nuclear double resonance (ENDOR) studies on KDP-type crystals have been collected in a recent review [1]. So, EPR studies have been carried out on several iron group impurities like Cu^{2+}, Mn^{2+}, Fe^{3+}, Cr^{5+} [1] and Cr^{3+} [1–3]. The structural results of these EPR works indicate that the impurity always enters the K^+ or NH_4^+ sites of KDP, DKDP, and ADP, except for Cr^{5+}, which is located in P^{5+} and As^{5+} tetrahedral sites. Charge compensation is mainly achieved by the loss of one (Cu^{2+}) or two (Cr^{3+}, Fe^{3+}) protons sited on oxygen bridges next to the impurity, as was inferred from the principal axes of the fine structure tensors (see figure 1 for the Cr^{3+} defect reported in [3]). As a consequence of the KDP lattice symmetry (space group, $I\bar{4}2d$), there are eight magnetically inequivalent sites for Fe^{3+} and Cr^{3+}, the directions of the defect principal axes being related by the point group $\bar{4}2m$. (See, for example, [4] for the structure of KDP and a compilation of the refined structural parameters in KDP-type crystals at different temperatures.)

On the other hand, ionizing radiation originates free radicals like OPO_3H^- and $OOP(OH)_2$ in KH_2PO_4, or AsO_4^{4-} in KH_2AsO_4 [1], due to the loss of a proton and/or loss/capture of one electron; in most of these cases the ENDOR technique has been decisive for the right identification of the radicals. ENDOR spectroscopy has been also employed to study the Cr^{5+} impurity [1], but as far as we know, ENDOR studies of the impurities located on K^+ or NH_4^+ sites have not been reported.

In this work the ENDOR spectra of Cr^{3+} in KDP have been measured in order to investigate the magnetic interaction of the Cr^{3+} ion with the neighbouring protons,

0953-8984/92/092297 + 12 $04.50

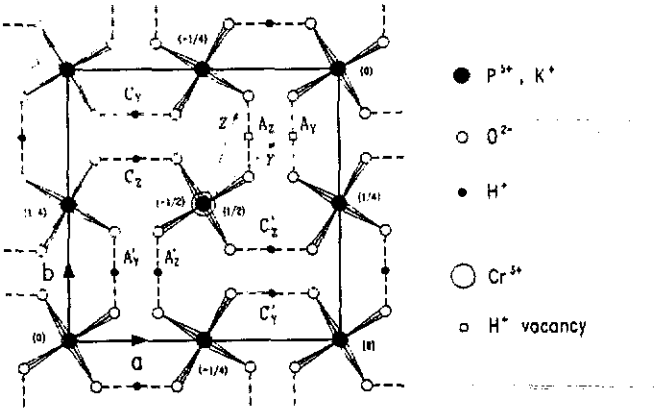

Figure 1. Projection of the structure of KDP at room temperature in the *ab* plane. The large square represents the unit cell, with dimensions: $a = b = 7.4521$ Å, $c = 6.974$ Å, after [4]. Fractional coordinates along the crystallographic *c* axis are given for the P^{5+} ions. The K^+ ions are aligned with the P^{5+} ions and displaced half the lattice parameter along *c*. P–O bonds are drawn in perspective. The defect A reported in [3] has also been schematized, showing the Cr^{3+} ion at the K^+ site located at $c = 0$, as well as the fine structure tensor axes *Z* and *Y* and the two proton vacancies. The eight nearest neighbour proton positions of Cr^{3+} are labelled A_Z, ..., C'_Y, and their coordinates are given in table 2.

which was not observed in the EPR spectra, and to obtain structural information. In addition, this study allows us to check the defect models proposed in [2, 3] from the EPR works.

2. Experimental details

A Cr-doped KDP crystal was grown by slowly cooling a saturated aqueous solution to which $CrCl_3$ was added. A sample with the appropriate dimensions (about 3.5 mm × 3.5 mm × 3 mm) was sawn from the whole prism. The natural growth faces were used as an indication of the crystallographic axes *a*, *b* and *c*.

The sample used in this work presents both the Cr^{3+} EPR spectrum reported by Kobayashi [2] as well as the Cr^{3+} EPR spectrum described by Bravo *et al* [3]. The latter shows more intense EPR lines than the former. In [3] it was concluded that both EPR spectra are owing to similar orthorhombic centres (Cr^{3+} in the K^+ site and the same two proton vacancies) but they present slightly different fine structure tensors. The first one was assigned to the 'regular' regions of KDP (R-defect) and the second one to the 'growth bands' regions (GB-defect), which present slightly larger lattice parameters [3, 5]. In this work we have studied the ENDOR spectra of the GB-defect.

The ENDOR spectra have been recorded at 4.2 K with a modified Varian E-1700 ENDOR spectrometer. This apparatus employs a 20 W broadband amplifier (ENI 420L) loaded by a three-turn coil (0.15 μH) placed inside the H_{102} microwave cavity (X band). The loaded *Q* of this cavity is about 6000. A modulation of the RF field (range 0.1–160 MHz) saturating the NMR transitions was employed without any additional modulation of the static magnetic field. The ENDOR spectra were measured with both amplitude and frequency modulation (Δf mode) of the saturating RF field [6]. In the

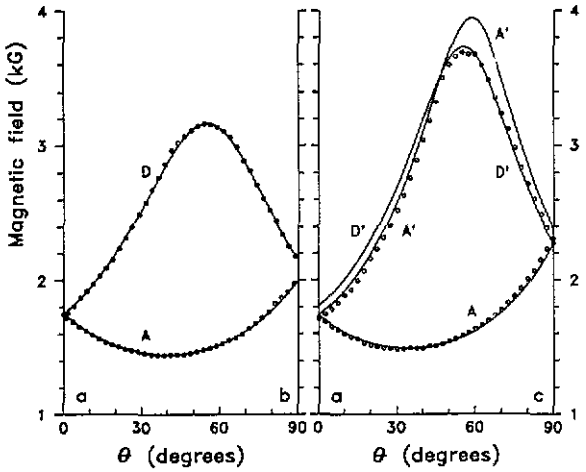

Figure 2. EPR angular variations of the $|-3/2\rangle \rightarrow |-1/2\rangle$ electronic transition at 4.2 K near the planes *ab* and *ac* of KDP, for the defects A, A', D, D'. Circles represent the values of the magnetic field for which ENDOR spectra have been measured. Full curves show the theoretical fitting obtained with the spin-Hamiltonian parameters reported in [3], except for a slightly different D parameter (see text).

Δf mode (differential pulse method) the RF signal from the frequency synthesizer is frequency modulated at 1 kHz and fed to the RF gate. The gate chops the frequency-modulated signal, but at 2 kHz. The difference in frequency of the pulses is constant (Δf) as the average radiofrequency is swept. ENDOR signals, such as the derivative of an absorption line, are observed.

3. Results and discussion

3.1. EPR and ENDOR spectra

At 4.2 K KDP is ferroelectric (space group, *Fdd*2) and the EPR spectrum undergoes remarkable changes with respect to the room temperature spectrum. Due to the presence of two different types of ferroelectric domains the number of EPR lines is doubled [5]. Such kinds of changes below the transition temperature have been observed in other EPR spectra of paramagnetic defects on KDP and its isomorphs [7, 8]. They have been explained by the appearance of two magnetic interaction tensors, each one related to one domain.

For this ENDOR study it is necessary to know the changes of the $\hat{D}$ tensor with temperature and to know accurately the orientation of the sample. To this aim, room- and low-temperature EPR measurements were performed in the ENDOR cavity for the GB-defects in one of the domains. Figure 2 shows the EPR angular variations measured at 4.2 K of the $|-3/2\rangle \rightarrow |-1/2\rangle$ electronic transition. A good fitting of these angular variations is obtained by using the same principal axes (X,Y,Z) of the defect as for room temperature measurements [3] (this is also observed for Fe^{3+} in KDP in the ferroelectric phase [8]) and a different value of the D parameter (D(300 K) = 13104 MHz, D(4.2 K) = 14066 MHz). This study allows us also to know accurately the orientation of the sample.

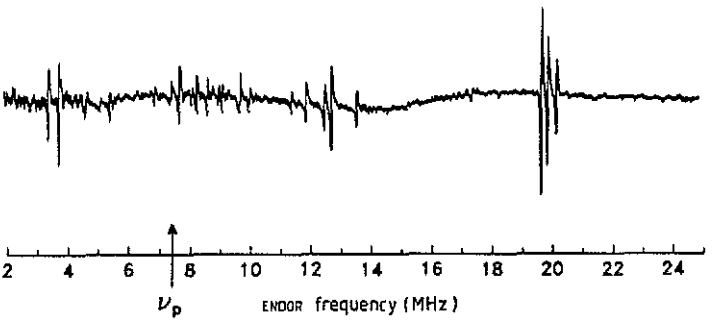

Figure 3. First derivative ENDOR spectrum obtained for a magnetic field value of 1739 G. The magnetic field orientation corresponds to $\theta = 67.5°$ in the angular variation *ac* of figure 2. The arrow indicates the Larmor frequency of protons ν_p.

The angular variations were very close to the *ab* and *ac* planes. From the intensity ratio of the EPR lines at 4.2 K the sign of the *D* parameter was determined to be positive.

The angular dependences of the ENDOR spectra were measured near the *ab* and *ac* planes of the KDP crystal for the above mentioned electronic transition. As can be observed in figure 3, the ENDOR spectra basically consist of three regions: (i) a set of lines appearing at frequencies higher than the proton Larmor frequency, (ii) another one at smaller frequencies and (iii) a central region with many overlapped lines around this Larmor frequency, where it is difficult to follow the whole angular variation of the ENDOR lines. At first glance, the ENDOR lines with the higher and smaller frequency values should correspond to the closest protons ($I = 1/2$) to Cr^{3+}, and the central region to the second closest and more distant nuclei. The ENDOR linewidths are about 50 kHz. Figures 4(*a*) and 4(*b*) show the angular dependence of the ENDOR frequencies near the *ab* and *ac* planes of KDP, corrected for the proton Larmor frequency corresponding to the applied magnetic field.

Moreover, it is necessary to take into account that the phosphorus nuclei ($I = 1/2$) around the Cr^{3+} ion can also give rise to ENDOR lines in the same frequency regions. Therefore, we have measured the ENDOR line positions, in dependence of the magnetic field, in order to assign the ENDOR lines to the different sorts of nuclei. Because of the broad EPR lines of the Cr^{3+} centres this was done by recording ENDOR spectra for different magnetic field values around the original magnetic field. The procedure was repeated for different orientations of the magnetic field. For most of the lines we have obtained a frequency shift of about $4\,kHz\,G^{-1}$, which is typical for ENDOR lines of protons. However, for several lines the shift was about $2\,kHz\,G^{-1}$, typical for lines of phosphorus nuclei. In Figures 4(*a*) and 4(*b*) the lines coming from phosphorus have been labelled P.

On the other hand, owing to the high number of lines in the EPR spectra (there are 16 different GB-defects and 16 R-defects, every one giving rise to up to four EPR lines), many ENDOR signals can be considered as 'satellite' signals, because they do not correspond to the single EPR line for the one domain we are studying. However, full angular variation of the ENDOR lines is observed in figure 4 only for the EPR lines which are very close to the studied line and have a very similar EPR angular dependence. Such close and 'parallel' EPR lines mainly come from the second domain of the GB-defects, but also from both domains for the R-defects. This explains the presence of two, three or four lines in the ENDOR angular variations showing a similar angular dependence. In figure 4, label

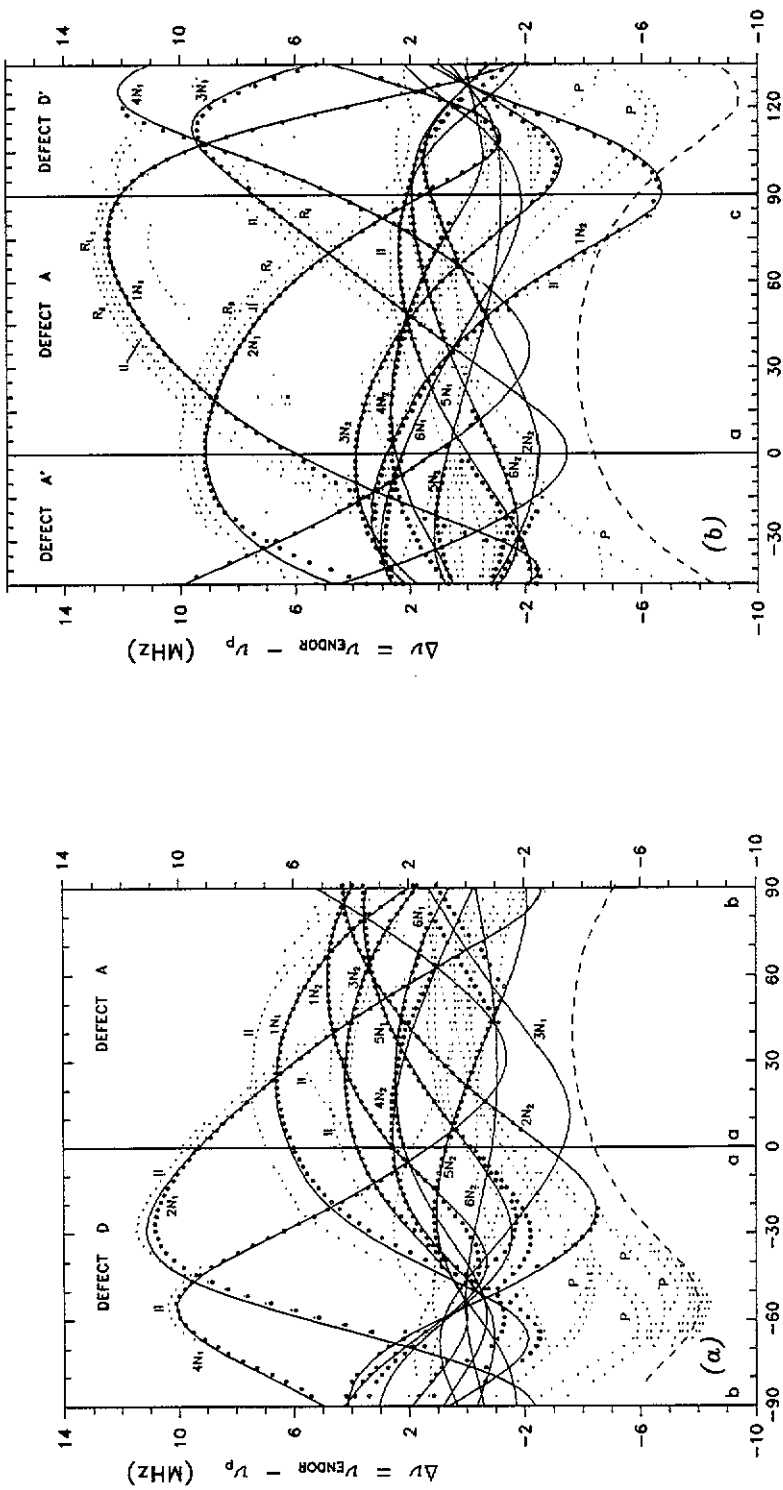

Figure 4. ENDOR angular variations at 4.2 K near the *ab* (*a*) and *ac* (*b*) planes of KDP, obtained for the magnetic field values shown in figure 2. Labels $1N_1$, $1N_2$, ..., $6N_2$ refer to the ENDOR transitions occurring in the electronic levels $|-3/2\rangle \equiv N_1$ and $|-1/2\rangle \equiv N_2$ for protons 1, ..., 6. These labels correspond to the theoretical fittings (full curves) of the experimental ENDOR lines (circles). Dots represent other experimental ENDOR lines observed (see text for explanation). Broken curves correspond to the Larmor frequency of phosphorus in this representation.

II stands for the second-domain lines of the GB-defect, and labels R_I and R_{II} for both domains of the R-defect. The circles in figure 4 represent ENDOR lines corresponding to the first domain of the GB-defect we have studied, which were the more intense lines, as seen in figure 3.

In order to analyse the ENDOR angular variations for the proton lines the following spin-Hamiltonian has been considered ($S = 3/2$ for Cr^{3+} and $I = 1/2$ for protons):

$$H = \beta \boldsymbol{B} \cdot \hat{\boldsymbol{g}} \cdot \boldsymbol{S} + D[Sz^2 - (1/3)S(S+1)] + E(Sx^2 - Sy^2)$$
$$- \sum_{p=1}^{m} g_n^p \beta_n \boldsymbol{B} \cdot \boldsymbol{I}^p + \sum_{p=1}^{m} \sum_i \sum_j A_{ij}^p S_i I_j^p \qquad (i,j = X, Y, Z). \tag{1}$$

This spin-Hamiltonian has been expressed in the defect principal axes system (X, Y, Z) where $\hat{\boldsymbol{g}}$ and $\hat{\boldsymbol{D}}$ tensors are diagonal. In order to relate the crystallographic axes (a,b,c) to the defect axes system, Eulerian angles have been used [2, 3]. The three first terms of (1) correspond to the EPR Hamiltonian, which was solved in [3]. The fourth term represents the nuclear Zeeman interactions with m protons which surround Cr^{3+} in the magnetic field $\boldsymbol{B}$ (we have assumed an isotropic nuclear g_n factor). Finally, the last term expresses the ligand hyperfine interactions of Cr^{3+} with the m protons. We assume that the superhyperfine interaction tensors are symmetric.

In order to evaluate the A_{ij}^p components of the $\hat{\boldsymbol{A}}$ tensor for each proton from the experimental ENDOR frequencies, we have numerically diagonalized the spin-Hamiltonian (1) for each of the m systems consisting of Cr^{3+} and one proton. This approximation is good because the direct and indirect nuclear–nuclear dipole interactions are weak. Such a procedure allows us to calculate the ENDOR frequencies for each value and orientation of the magnetic field, depending on the set of six A_{ij}^p parameters. Four ENDOR frequencies are obtained, which correspond to the $|-1/2\rangle \rightarrow |1/2\rangle$ nuclear transition of the proton occurring in each of the four Cr^{3+} electronic levels. However, as we have studied the EPR transition $|-3/2\rangle \rightarrow |-1/2\rangle$, only two of the four frequencies are observed in the ENDOR spectra (figures 4(a) and 4(b)). Furthermore, a least square fit method has been used to evaluate the different sets of six A_{ij}^p components. The frequency values obtained whenever the fitting process is concluded are plotted as a full line in figures 4(a) and 4(b). From these angular variations, only the fits for the so-called 'A-defect' have been made (figure 2). Next, the ENDOR lines have been calculated for all experimental frequencies to check for the goodness of the different fits. In general, good agreement has been obtained in all cases, the small differences being probably due to the values employed for the parameters D and E, as well as for the Eulerian angles.

The more intense ENDOR lines in the angular variations are described by the interaction with six protons whose hyperfine tensors are given in table 1. The tensors have been diagonalized and the principal values have been decomposed into their isotropic and anisotropic parts. Their signs have been determined to be positive according to the positive sign of the D parameter. The principal axes x, y and z have been expressed in the (a, b, c) system for the A-defect. Errors in the principal values have been obtained from the least square fit method by considering an experimental uncertainity of 0.05 MHz in the ENDOR line position; errors in the principal axes come also from an uncertainty of 0.5° in the Eulerian angles. The actual errors for the tensor associated with proton 5 could be larger than those presented in table 1 because the ENDOR transitions N_2 fall into the central region of the spectra, and the strong overlapping makes it difficult to follow the whole angular variation of this line.

Table 1. Proton hyperfine tensors decomposed in their isotropic A_{iso} and anisotropic B_{ii} parts (in MHz). θ and φ coordinates refer the principal axes (x, y, z) of the tensor to the crystallographic axes (a, b, c). The x, y and z axes correspond to defect A according to figure 1. Errors in the coordinates for x and y axes range around ±5°.

Proton	A_{iso}	$B_{ii}, i = x, y, z$	θ (degrees)	φ (degrees)
		−5.12 ± 0.12	83	232
1	3.39 ± 0.09	−4.67 ± 0.08	107	320
		9.79 ± 0.08	19 ± 1	342 ± 2
		−4.11 ± 0.09	63	74
2	2.41 ± 0.12	−3.80 ± 0.15	148	40
		7.91 ± 0.12	105 ± 2	156 ± 1
		−4.21 ± 0.80	101	215
3	2.13 ± 0.44	−4.80 ± 0.25	73	302
		9.01 ± 0.29	20 ± 1	158 ± 2
		−7.21 ± 0.15	58	276
4	5.58 ± 0.26	−1.14 ± 0.47	120	206
		8.35 ± 0.17	134 ± 3	329 ± 1
		−4.01 ± 0.30	86	342
5	−1.00 ± 0.16	−0.30 ± 0.12	35	246
		4.31 ± 0.11	125 ± 2	255 ± 2
		−1.78 ± 0.10	151	192
6	0.60 ± 0.14	−1.31 ± 0.07	98	297
		3.09 ± 0.03	62 ± 3	212 ± 3

3.2. Analysis of the proton hyperfine tensors

3.2.1. Isotropic constants. First of all, the values for the isotropic constants A_{iso} in table 1 allow the calculation of the unpaired spin density present in the 1s hydrogen orbital. Such values correspond to the fractions 0.24%, 0.17%, 0.15%, 0.39%, −0.07% and 0.04% for protons 1, 2, 3, 4, 5, and 6, respectively. As observed by Dalal *et al* for the AsO_4^{4-} centre in KH_2AsO_4 [9], it is likely that the mechanism for this isotropic interaction is the same as in free radicals, i.e. the exchange polarization of the O–Hσ bond by the spin density on one of the oxygens of the bridge. Moreover, as the isotropic constants are mainly positive, the exchange polarization mechanism implies that the electron spin density on the oxygens should be negative (β spin) [10]. Such a β spin on oxygen would be transferred mainly through the Cr–O bond. Besides, the spin density on chromium should have the contrary sign, as observed in general for this bond [11], i.e. it should be positive (α spin). On the other hand, B_{zz} (the largest anisotropic component) is found to be positive for all protons, which is in agreement with an anisotropic interaction, dominantly dipolar in nature.

3.2.2. Axial anisotropic tensors. As can be observed in table 1, protons 1, 2, 3 and 6 present almost axial anisotropic hyperfine tensors. This fact can be interpreted as a dipole–dipole interaction between the unpaired electron spin in the Cr^{3+} and the point nuclear spin of these protons. Therefore, this interaction allows us to locate such protons

Table 2. Polar coordinates of the $K^+ - H^+$ directions in the crystallographic system (a, b, c) and distances for the eight nearest protons of a K^+ ion in the pure KDP lattice at room temperature [4], according to figure 1.

Proton	K^+–H^+ direction		K^+–H^+ distance (Å)
	θ (degrees)	φ (degrees)	
A_Z	140.2 ± 0.1	59.4 ± 0.1	
A'_Z	140.2 ± 0.1	239.4 ± 0.1	3.38 ± 0.01
C_Z	39.8 ± 0.1	149.4 ± 0.1	
C'_Z	39.8 ± 0.1	329.4 ± 0.1	
A_Y	74.8 ± 0.1	35.4 ± 0.1	
A'_Y	74.8 ± 0.1	215.4 ± 0.1	3.32 ± 0.01
C_Y	105.2 ± 0.1	125.4 ± 0.1	
C'_Y	105.2 ± 0.1	305.4 ± 0.1	

around Cr^{3+}. Besides, they should be nearest-neighbour protons because they give rise to the highest frequency ENDOR lines observed.

The polar coordinates and the lengths of the $(K^+–H^+)$ vectors of the eight nearest neighbour protons of K^+ in the pure KDP lattice are given in table 2 for comparison. It is observed that protons 1, 2, 3 and 6 can be reasonably assigned to protons C'_Z, C_Y, C_Z and A'_Y, respectively, in spite of the considerable differences between the original directions (table 2) and the measured ones (table 1). Although, in table 2, the coordinates for the pure KDP lattice at room temperature are given, the ionic positions do not change too much in the ferroelectric phase [4]. The main well-known changes are the two different positions for each proton in the bridge (which originate both ferroelectric domains), but these cannot explain the differences observed. Therefore, the more important structural changes must be attributed to the Cr^{3+} ion.

In order to confirm that these protons are nearest neighbours of the paramagnetic Cr^{3+} ion and to get information about the distortion, we use the point-dipole approximation to estimate the effective electron–nuclear separation R. In this approximation, the anisotropic hyperfine constant B_{zz} is given by

$$B_{zz} = 2gg_n^p\beta\beta_n(1/R^3) \tag{2}$$

where $\beta\beta_n = 7.069$ MHz Å^3. Using this expression we obtain $R = 2.53$, 2.71, 2.60 and 3.71 Å for protons 1, 2, 3 and 6, respectively. Thus, these protons must be the first neighbours of Cr^{3+} because the distances for the eight first-neighbour protons of the potassium site in the pure KDP lattice are 3.32 and 3.38 Å, whereas the second-neighbour protons are 4.87 and 5.25 Å away from such a site.

The calculated distances indicate that protons C'_Z, C_Y and C_Z have approached the Cr^{3+} ion by about 0.7 Å, whereas proton A'_Y has moved away by about 0.4 Å. This result is in agreement with the strong distortion of the lattice around Cr^{3+} concluded from the EPR studies [2, 3]. However, those calculated distances are expected to be underestimated due to the point-dipole approximation.

3.2.3. Orthorhombic anisotropic tensors. Protons 4 and 5 show orthorhombic anisotropic tensors (see table 1). Therefore, it is expected that the direction of their z principal axes does not locate the corresponding protons, as considered for the 1, 2, 3 and 6 protons in

the previous section. However, as a first approach the z axes can be used to assign tentatively protons 4 and 5 to protons C'_Y and A'_Z in figure 1 respectively (see table 2), because we expect the unpaired electron spin to be mainly localized in chromium [12], thus the axial Cr–H dipolar interaction should dominate over any other anisotropic interaction.

The origin for the orthorhombic character of these tensors would be similar to the one considered by Dalal *et al* [9] for the AsO_4^{4-} centre in ADP; although, in this case, the unpaired spin density comes from one unpaired electron in the AsO_4 group. In our case the mechanism consists of two kinds of hyperfine interactions: (a) the axial dipolar interaction between Cr^{3+} and a proton, as detected for protons 1, 2, 3 and 6; and (b) the dipolar interaction of a substantial unpaired spin density on one oxygen (first neighbour of the Cr^{3+} ion and adjacent to the proton) with the nuclear spin of the proton [13, 14]. It follows that the orthorhombic tensors measured for protons 4 and 5 result from the addition of both interactions. Therefore, such tensors can be decomposed if the tensor associated with interaction (b) is calculated and subtracted from the total orthorhombic tensor. The result of such an operation should be an axial tensor corresponding to interaction (a) between chromium and proton 4 or proton 5, as obtained for the other protons. In order to calculate the tensor corresponding to interaction (b) the corrected Slater orbital formulas of McConnell and Strathdee [14, 15] have been employed. In our case, the following expressions for the principal values of this tensor have been used:

$$\begin{aligned}
A_{\xi\xi} &= 2(gg_n\beta\beta_n/R^3)[1 - 36/K^2R^2 + (K^3R^3/8 + K^2R^2 + 5KR + 17 + 36/KR \\
&\quad + 36/K^2R^2)e^{-KR}]\rho_\pi \\
A_{\eta\eta} &= -(gg_n\beta\beta_n/R^3)[1 - 18/K^2R^2 + (K^2R^2/4 + 2KR + 8 + 18/KR \\
&\quad + 18/K^2R^2)e^{-KR}]\rho_\pi \\
A_{\zeta\zeta} &= -(gg_n\beta\beta_n/R^3)[1 - 54/K^2R^2 + (K^3R^3/4 + \frac{7}{4}K^2R^2 + 8KR + 26 \\
&\quad + 54/KR + 54/K^2R^2)e^{-KR}]\rho_\pi
\end{aligned} \tag{3}$$

where $K = 8.41$ Å^{-1} for oxygen, R is the distance between oxygen and the proton, and ρ_π represents the unpaired electron spin fraction in the $2p\pi$ orbitals of oxygen.

In (3) the principal axes ξ, η and ζ are centred on the oxygen, and are determined by the direction O–H (ζ axis) and the direction of one $2p\pi$ orbital lobe (η axis). We assume that the O–H directions (ζ axes) are the same as in pure KDP, and nearly coincide with the a or b crystallographic axes (figure 1). As we have tentatively assigned protons 4 and 5 to protons C'_Y and A'_Z respectively (figure 1), for the case of proton 4 (5) the ζ axis is coincident with the crystallographic a axis (b axis). This choice confines the η axis to the crystallographic bc (ac) plane, so that its direction can be obtained by means of a single parameter δ. This parameter can be defined as the angle of the η axis with the crystallographic c axis, its values ranging from $\delta = -90°$ (η pointing along the $-b$ or $-a$ directions) to $\delta = +90°$ (η pointing along the $+b$ *or* $+a$ directions).

Thus, in order to construct the anisotropic O–H tensor with expressions (3), we have to choose R, ρ_π, and δ. These three parameters must satisfy the condition that the tensor corresponding to interaction (a) must be an axial tensor. This is performed by translating the tensors to the (a,b,c) crystallographic axes system. Since, in pure KDP, distances R are 1.05 and 1.43 Å for the two positions of the proton in the bridge, we have considered reasonable values for R, ranging from 0.5 to 1.8 Å. It was found for protons 4 and 5 that

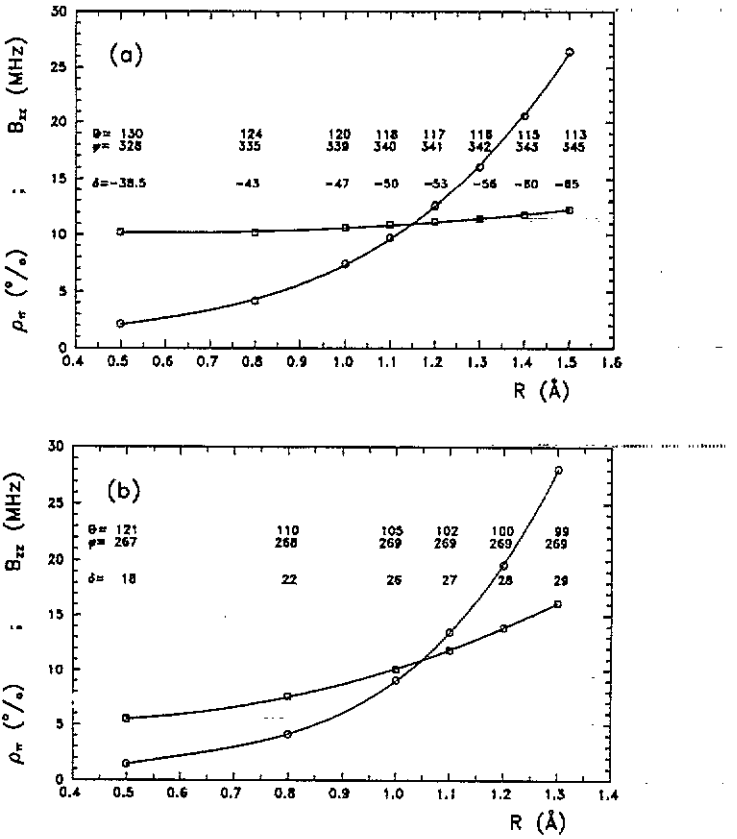

Figure 5. Unpaired spin fraction ρ_π (○) in the oxygens and B_{zz} component (□) of the resulting axial tensors for protons 4 (*a*) and 5 (*b*) as a function of the distance R between oxygen and the proton. The polar coordinates θ and φ (degrees) for the z axis of the axial tensors refering to the crystallographic (a, b, c) system and the corresponding angle δ are given aligned with each point.

only one pair of values (ρ_π,δ) make the resulting tensor accurately axial for each value of R. In figure 5 the results of the decomposition for protons 4 and 5 are presented. In both cases the sign of the ρ_π electron spin density must be taken as negative (β spin) to obtain axial tensors. Moreover, the resulting B_{zz} components for the axial tensor are positive, as obtained for the tensors of protons 1, 2, 3 and 6. The negative spin density in the oxygen agrees with the positive isotropic constant measured for proton 4, according to the exchange–polarization mechanism [10], but is not in agreement with the negative isotropic constant determined for proton 5. However, for this proton, the indetermination of its hyperfine parameters can be higher than the errors given in table 1, as explained above; and therefore, the sign of the isotropic constant is not clear.

As observed in figure 5(*a*), the B_{zz} component of the Cr–H axial tensor for proton 4 is similar to the measured ones for protons 1, 2 and 3 in a wide range of R. On the other hand, the unpaired spin density obtained for proton 4 as a function of the distance R can be compared with the results obtained by Dalal *et al* [9]. These authors consider the so-called 'close' protons being at a distance R = 1.06 Å and estimate a fraction 16% of the unpaired spin density on each oxygen of the AsO_4^{4-} centre, the isotropic constant

corresponding to a fraction 0.97% of the unpaired electron in the 1s hydrogen orbital. In our case, for a distance $R \approx 1$ Å the obtained spin density on oxygen is about 7%, and a fraction 0.39% of the unpaired electron in the 1s hydrogen orbital has been measured for proton 4. One can observe that the ratio 7/0.39 determined here agrees very well with the ratio 16/0.97 obtained in [9]. So, we propose that proton 4 is separated by around 1 Å from the first-neighbour oxygen of Cr^{3+}. The corresponding polar coordinates in figure 5(*a*) allow us to assign proton 4 to proton C'_Y in figure 1.

The results for proton 5 in figure 5(*b*) are not as clear as for proton 4, but the values obtained for B_{zz} are reasonable and positive, being similar to those of protons 1, 2, 3 and 4 for distances around 1 Å. The values for the spin densities on the oxygen are also reasonable. On the other hand, the other possible positions for proton 5 have also been considered, i.e. protons A_Z and A_Y in figure 1. These correspond to the vacancies proposed in the EPR works [2, 3]. For these two cases, accurate decomposition of the orthorhombic tensor for proton 5 is also possible, but the values obtained for the highest component of the axial tensor (B_{zz}) are negative. This result contradicts the positive sign of such a component for an axial dipolar interaction with protons. Therefore, as proton 5 should be a first neighbour of Cr^{3+} and there are no more options, it is finally assigned to proton A'_Z in figure 1.

4. Conclusions

In the former sections the proton hyperfine tensors 1, 2, 3, 4, 5 and 6 have been assigned to the protons C'_Z, C_Y, C_Z, C'_Y, A'_Z and A'_Y, respectively, for the A-defect (figure 1). Therefore, our results agree with the EPR model [2, 3] for the defect, i.e. Cr^{3+} substituting for K^+ with proton vacancies at the positions A_Z and A_Y. Moreover, there are some lines near the central region of the ENDOR spectra which are not assigned to any first-neighbour proton. It is believed they come from second-neighbour protons which are closer to the Cr^{3+} ion than in the pure KDP lattice, because of the distortion of its surroundings.

On the other hand, some considerations about the neighbourhood of the impurity can be made: if protons A_Z and A_Y (figure 1) are lost, a repulsion between the oxygens of the broken bridges should exist. This repulsion would lead to a rotation around the crystallographic *c* axis of the affected PO_4 tetrahedra, as measured by Tsuchida *et al* [16] and later by Wells *et al* [13] from a broken bridge in KDP. Thus, it would be expected that protons A'_Z, C_Y and C'_Z experience a strong position change, whereas protons C_Z and C'_Y experience it to a lower extent, the proton A'_Y being hardly affected. Comparing tables 1 and 2, it is observed that proton A'_Y presents the lowest change in the Cr–A'_Y direction, in agreement with the former arguments. Besides, the estimated increase in the distance for proton A'_Y can be understood if the Cr^{3+} ion is displaced towards the proton vacancies due to their net negative charge.

References

[1] Müller K A 1987 *Ferroelectrics* **72** 273–304
[2] Kobayashi T 1973 *J. Phys. Soc. Japan* **35** 558–72
[3] Bravo D, López F J, Diéguez E, Aguilar M and Cabrera J M 1989 *J. Phys.: Condens. Matter* **1** 6145–51
[4] Nelmes R J, Tun Z and Kuhs W F 1987 *Ferroelectrics* **71** 125–41
[5] Bravo D, López F J and Gonzalo J A 1989 *J. Phys.: Condens. Matter* **1** 9791–3

[6] Hyde J S 1965 *J. Chem. Phys.* **43** 1806–18
[7] Kawano T, Niimori K, Hukuda K and Fujita N 1970 *J. Phys. Soc. Japan* **29** 633–42
[8] Tsuchida K and Abe R 1979 *J. Phys. Soc. Japan* **46** 1225–31
[9] Dalal N S, McDowell C A and Srinivasan R 1972 *Mol. Phys.* **24** 417–39
[10] Carrington A and McLachlan A D 1979 *Introduction to Magnetic Resonance* (London: Chapman and Hall) ch 6
[11] Geschwind S 1972 *Electron Paramagnetic Resonance* (New York: Plenum Press) ch 8
[12] Schweiger A and Günthard H 1978 *Chem. Phys.* **32** 35–61
[13] Wells J W, Budzinski E and Box H C 1986 *J. Chem. Phys.* **85** 6340–6
[14] McConnell H M and Strathdee J 1959 *Mol. Phys.* **2** 129–38
[15] Box H C, Budzinski E and Potienko G 1978 *J. Chem. Phys.* **69** 1966–70
[16] Tsuchida K, Abe R and Naito M 1973 *J. Phys. Soc. Japan* **35** 806–9